CMS Physics Analysis Summary

Contact: cms-pag-conveners-heavyions@cern.ch 2024/06/11

Elliptic anisotropy at high p_{T} in pPb collisions using subevent cumulants

The CMS Collaboration

Abstract

The second-order (elliptic) Fourier coefficients (v_2) as a function of particle transverse momentum (p_{T}) and event multiplicity are presented for pPb collisions using a subevent multiparticle cumulant analysis where nonflow effects are strongly suppressed. The data were recorded by the CMS experiment at a nucleon-nucleon center-of-mass energy of $\sqrt{s_{\mathrm{NN}}} = 8.16$ TeV. The new measurement probes an extended range of particle p_{T}, up to values where the influence of nonflow effects are shown to strongly influence the results using a standard cumulant analysis. Results for both pPb and PbPb collisions are compared in similar multiplicity ranges, allowing for an assessment of the medium influence on the elliptic anisotropy associated with high p_{T} particle production.

The observation of strong collective azimuthal correlations in relativistic nucleus-nucleus (AA) collisions at the BNL RHIC [1–3] and CERN LHC [4–9] facilities is believed to reflect the formation of a quark-gluon plasma (QGP) that exhibits nearly ideal hydrodynamic behavior [10–12]. The azimuthal correlation structure of the emitted particles can be characterized by its Fourier components. In hydrodynamic models, the second and third Fourier components, known as elliptic (v_2) and triangular (v_3) flow, respectively, reflect the response of the medium to the initial collision geometry and fluctuations, providing insights into the fundamental transport properties of the QGP medium [13, 14]. Similar correlations have been observed in high-multiplicity proton-lead (pPb) [15–18] collisions at the LHC, which raises the question of whether a fluid-like QGP state is also created in small hadronic collision systems. These long-range correlations have also been studied in lighter AA systems such as dAu [19, 20] and ^{3}HeAu [21] at RHIC, with the properties of the observed long-range correlations in small systems consistent with hydrodynamic models of a tiny QGP droplet [22].

The present analysis focuses on the origin of azimuthal anisotropy at very high transverse momentum(p_T). At high p_T, partons are not expected to be thermalized in the hot and dense medium created in heavy ion collisions, and a hydrodynamic picture is not applicable. Rather, the observed azimuthal anisotropy in this regime is primarily attributed to the interaction between high-p_T partons and the QGP medium [23, 24], which is expected to have a lenticular geometry for non-central AA collisions. As the high-p_T partons traverse through the hot and dense medium, they lose energy through induced radiation and collisional interactions with the medium constituents. This energy loss depends on the path length traversed by the partons through the medium, which in turn depends on the direction in which the partons travel relative to the orientation of this medium [25–28].

The evidence for the formation of a QGP in pPb collisions [29, 30] makes the study of how this smaller scale medium affects high-p_T partons of considerable interest. The azimuthal correlations of high-p_T particles in small system collisions has been previously studied, e.g., in Refs. [31, 32], using a two-particle correlation technique. To remove short-range, nonflow correlations, these analyses have used either peripheral subtraction or template fit methods [33], which are based on the strong assumption that peripheral events have negligible contribution from the extended medium. The method used in the present analysis is based on the Q-cumulant multiparticle correlation technique [34] with subevents [35, 36]. Rapidity gaps are required between the particles in the correlators to strongly suppress short-range correlations. This note presents the first subevent cumulant analysis of the azimuthal anisotropy up to $p_T \sim 20$ GeV in pPb collisions at $\sqrt{s_{\mathrm{NN}}} = 8.16\,\mathrm{TeV}$. The results are compared to a similar analysis using PbPb collision events at $\sqrt{s_{\mathrm{NN}}} = 5.02\,\mathrm{TeV}$. Both collision systems were measured using the CMS experiment at the LHC.

The CMS detector is composed of various subsystems, one of which is the silicon tracker. This tracker is situated within the 3.8 T field of a superconducting solenoid and consists of 1440 silicon pixel and 15,148 silicon strip detector modules (Phase-0). In 2017, the pixel detector received an upgrade with an additional layer added to both the barrel and endcap regions, resulting in an increased number of silicon pixel modules to 1856 (Phase-1) [37]. Charged particles within the laboratory pseudorapidity range $|\eta| < 2.5$ are measured by the silicon tracker, which provides transverse impact parameter resolutions of 25–90 (20–75) μm for Phase-0 (Phase-1) pixel detectors and a p_{T} resolution better than 1.5% up to 100 GeV [38]. The ECAL and HCAL calorimeters are also located inside the solenoid and cover the range $|\eta| < 3.0$. The ECAL utilizes lead tungstate crystals arranged in a quasi-projective geometry, while the HCAL barrel and endcaps are composed of brass and scintillator plates. The steel and quartz-fiber Cherenkov HF hadron forward calorimeters cover the range $2.9 < |\eta| < 5.2$ on either side of

the interaction region. The HF calorimeters are azimuthally divided into 20° modular wedges and further segmented to form 0.175×0.175 radians ($\Delta\eta\times\Delta\phi$) towers. The response of the CMS detector is simulated in detail using GEANT4, and a more comprehensive account of the CMS detector can be found in Ref. [39].

The measurements presented in this note use CMS data sets of 8.16 TeV pPb collisions and 5.02 TeV PbPb collisions taken in 2016 and 2018 and with integrated luminosities of 186 and $0.607\,\mathrm{nb}^{-1}$, respectively [40, 41]. For pPb collisions, the beam energies for protons and lead nuclei were 6.5 TeV and 2.56 TeV per nucleon pair, respectively, resulting in a center-of-mass energy of $\sqrt{s_{_{\mathrm{NN}}}} = 8.16\,\mathrm{TeV}$. A mid-run reversal of the beam directions had negligible effects on detector-related systematic effects, and the merged results are reported using the convention that the proton-going direction defines positive pseudorapidity.

To select high-multiplicity pPb collisions, a dedicated high-multiplicity trigger was implemented using CMS level-1 [42] and high-level trigger systems [43]. At level-1, events were triggered by requiring at least one track with $p_{\mathrm{T}} > 0.4\,\mathrm{GeV}$ in the pixel tracker during a pPb bunch crossing and at least one tower in one of the two HF detectors having an energy above 1 GeV. Additionally, the total number of ECAL and HCAL towers with transverse energies above a threshold of 0.5 GeV needed to exceed 120 and 150 in ECAL and HCAL, respectively. Events passing the L1 trigger were subsequently filtered by the HLT. To trigger minimum bias (MB) pPb events, at least one of the two hadronic forward (HF) calorimeters must register energy deposits above a threshold of around 1 GeV. Additionally, there must be at least one track with $p_{\mathrm{T}} > 0.4\,\mathrm{GeV}$ in the pixel tracker. Offline, events must also have a primary vertex within 15 cm of the nominal interaction point along the beam axis and 0.2 cm in the transverse direction. At least two reconstructed tracks must be associated with the primary vertex. Results are reported in ranges of $\mathrm{N}_{\mathrm{trk}}^{\mathrm{offline}}$, with $\mathrm{N}_{\mathrm{trk}}^{\mathrm{offline}}$ corresponding to the measured track multiplicity with $p_{\mathrm{T}} > 0.4\,\mathrm{GeV}$ and is not corrected for tracking efficiency. Table A.1 of the Appendix A reports the mean multiplicity $\langle \mathrm{N}_{\mathrm{trk}}^{\mathrm{offline}} \rangle$ and tracking efficiency corrected multiplicity $\langle \mathrm{N}_{\mathrm{trk}}^{\mathrm{corrected}} \rangle$ for various $\mathrm{N}_{\mathrm{trk}}^{\mathrm{offline}}$ ranges. An efficiency plateau above 95% is observed in the $\mathrm{N}_{\mathrm{trk}}^{\mathrm{offline}}$ range for the analysis.

The PbPb minimum bias (MB) events are selected based on signals surpassing readout thresholds in the range of ∼6–12 GeV on both sides of the HF calorimeters. The PbPb events are further filtered to have a primary vertex within 15 cm of the nominal interaction point along the beam axis and 0.2 cm in the transverse direction. Additionally, each HF detector must have at least two towers with a combined energy deposit of 4 GeV or more. The trigger, event reconstruction, and selections are described in previous correlation analyses [29, 44–46]. To perform correlation measurements, only primary tracks that originate at the primary vertex and meet the high-purity criteria of Ref.[38] are used for all data sets analyzed. The trigger and event selection efficiency was found to be about 98%. Furthermore, the impact parameter significance of the tracks with respect to the primary vertex in the longitudinal and transverse directions must be less than 3 standard deviations, and the relative p_{T} uncertainty must be less than 10% for the p_{T} range used in the analysis.

To ensure high tracking efficiency and minimal background contamination, only tracks with $|\eta| < 2.4$, $p_{\mathrm{T}} > 0.3\,\mathrm{GeV}$ (for pPb) and $p_{\mathrm{T}} > 0.5\,\mathrm{GeV}$ (for PbPb) are used in this analysis. The selected tracks are corrected for tracking inefficiency and acceptance using simulated Monte Carlo samples from HIJING v1.35 [47] and HYDJET 1.9 [48] for pPb and PbPb respectively, and the response of the CMS detector to these simulated events is based on GEANT4 [49]. In the measurement of correlations in pPb collisions, multiple independent interactions (pileup) in the same event may have constituted a background. The average number of collisions per

bunch crossing in the pPb data varied between 0.1 and 0.25. The procedure used for identifying and rejecting events with pileup was similar to that described in Ref. [44].

The multiparticle Q-cumulant [34] method is used to measure the v_2 value of charged hadrons within $|\eta| < 2.4$ using the software package *mcorrelations* [50]. The Q-cumulant method has been used to measure 4-, 6-, and 8-particle correlations in previous CMS publications [51, 52], with the multiparticle correlations being inherently less sensitive to the few-particle correlations such as those arising from jet fragmentation and back-to-back dijet correlations. In this method, the two- and four-particle correlators, $\langle\langle 2\rangle\rangle$ and $\langle\langle 4\rangle\rangle$ are defined as

$$\langle\langle 2\rangle\rangle = \langle\langle e^{in(\phi_1-\phi_2)}\rangle\rangle, \quad \langle\langle 4\rangle\rangle = \langle\langle e^{in(\phi_1+\phi_2-\phi_3-\phi_4)}\rangle\rangle. \tag{1}$$

Here, ϕ_j (j = 1, ..., 4) represents the azimuthal angles of four distinct particles in an event, and the notation $\langle\langle\cdots\rangle\rangle$ signifies that the average is calculated over all particles across all events. For elliptic flow, n = 2. Then the four-particle cumulant $c_n\{4\}$ is given as

$$c_n\{4\} = \langle\langle 4\rangle\rangle - 2\langle\langle 2\rangle\rangle^2, \tag{2}$$

which finally relates to the flow $v_n\{4\}$ as

$$v_n\{4\} = \sqrt[4]{-c_n\{4\}}. \tag{3}$$

The m-particle cumulant method correlates each Particle of Interest (POI) with $m-1$ Reference Flow Particles (RFPs). In this analysis, the RFPs for the cumulant method are charged hadrons within $|\eta| < 2.4$ and with $0.3 < p_T < 3.0$ GeV (for pPb) and $0.5 < p_T < 3.0$ GeV (for PbPb). The upper p_T bound of the RFP range is chosen so as to reduce the contribution of minijets, which can contribute above $p_T \sim 3$ GeV.

In a standard multiparticle Q-cumulant analysis, the POI and RFP ranges overlap in η. In order to suppress non-flow effect from the short-range correlations, a subevent method has been suggested based on the calculations published in Ref. [35]. It has to be noted that the method and calculation are essentially the same between the regular and subevent method, but for the subevent method instead of selecting particles in the full acceptance, particles are selected from different subevents to develop the cumulant values. By selecting the correlated particles from different subevents, the contribution from short-range correlations is naturally suppressed as a pseudorapidity gap is guaranteed between any two particles in a given correlation. To estimate the statistical uncertainties on the cumulants, we use the sub-group method in which the entire dataset is divided into six trials with comparable numbers of events. Using identical algorithms, the cumulants for each trial are calculated. The standard deviation of the resulting cumulant distribution is treated as a statistical uncertainty.

Figure 1 illustrates how we choose particle tracks to build our four particle correlators used in computing the cumulant values. The star(*) superscript is for the particles whose azimuthal angle has a negative sign in the correlator. The prime symbol denotes the POI. The top left case illustrates the case where four separate particles are chosen from the same pseudorapidity range. In this case, it is possible that all four particles will originate from a single jet, leading to a large nonflow contribution to the cumulant. In the top right panel, 2-subevent scenario, the probability to pick all particles in the same jet is small (particle a and b are chosen from distinct pseudorapidity range) and most remaining non-flow contribution comes from dijets. In the bottom left panel, the 3-subevent scenario is shown. In this case, the dijet contribution is drastically reduced since it is unlikely to select all four particles from the same dijet. Finally, in the 4-subevent scenario, each of the four particles is selected from distinct pseudorapidity

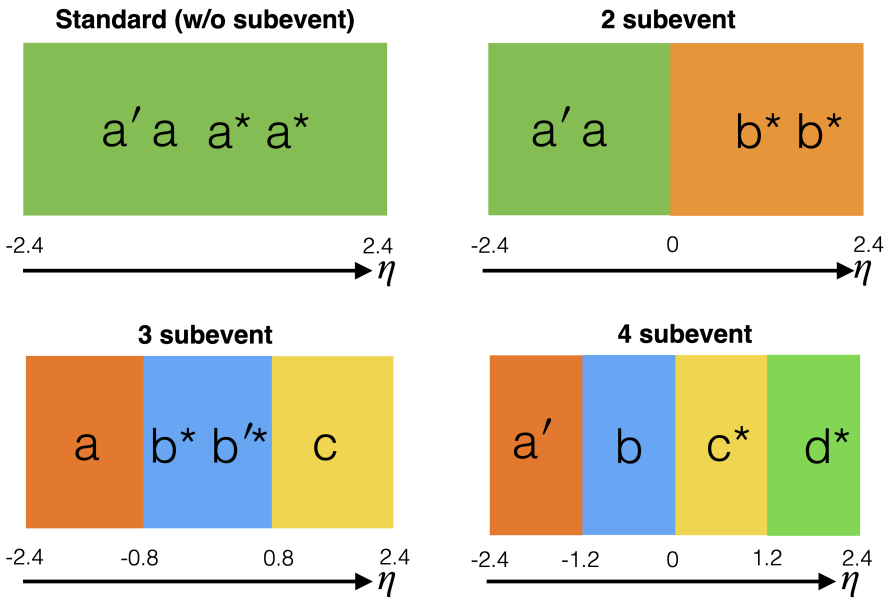

Figure 1: Subevent chosen in various cases in the CMS tracker acceptance to correlate four particles

ranges, further reducing the nonflow contribution.
In this analysis, we use p_T differential cumulants, $d_n\{4\}$, defined as

$$d_n\{4\} = \langle\langle 4' \rangle\rangle - 2\langle\langle 2' \rangle\rangle \cdot \langle\langle 2 \rangle\rangle, \tag{4}$$

where $\langle\langle 4' \rangle\rangle$ is 4-particle correlator with 3 RFPs and one POI and $\langle\langle 2' \rangle\rangle$ is 2-particle correlator with one RFP and one POI. In the following, we provide the formula to compute $d_n\{4\}$ in all scenarios, where a, b, c and d are refering to the particle chosen in a specific subevent and the symbol "|" indicates a separation between subevents. In Eq. 5, for example, the notation a′a|bb in the 4- particle correlator means that two particles are required to be in the first subevent (a′a) while the other two are required to be in the second subevent (bb), where a′ is the POI. Similarly, for the 2-particle correlator, one particle in each subevent is required (a′b).

The 2 subevent differential cumulant can be expressed in terms of the correlators with

$$d_n\{4\}_{2sub} = \langle\langle 4 \rangle^{a'a|b^*b^*} \rangle - 2\langle\langle 2 \rangle^{a'|b^*} \rangle \cdot \langle\langle 2 \rangle^{a|b^*} \rangle. \tag{5}$$

For the 3 subevent, the correlator expansion depends on the pseudorapidity range of POI, with

$$d_n\{4\}_{3sub} = \langle\langle 4 \rangle^{a|b^*b^*|c'} \rangle - 2\langle\langle 2 \rangle^{a|b^*} \rangle \cdot \langle\langle 2 \rangle^{b^*|c'} \rangle \tag{6}$$

when the POI is in the range $2.4 < |\eta| < 0.8$ and

$$d_n\{4\}_{3sub} = \langle\langle 4 \rangle^{a|b^*b'^*|c} \rangle - \langle\langle 2 \rangle^{a|b'^*} \rangle \cdot \langle\langle 2 \rangle^{b^*|c} \rangle - \langle\langle 2 \rangle^{a|b^*} \rangle \cdot \langle\langle 2 \rangle^{b'^*|c} \rangle \tag{7}$$

when $|\eta| < 0.8$. In the latter case, we have two choices for POI and accordingly two combinations for the product of 2-particle correlators ($\langle\langle 2 \rangle^{a|b'^*} \rangle \cdot \langle\langle 2 \rangle^{b^*|c} \rangle$ and $\langle\langle 2 \rangle^{a|b^*} \rangle \cdot \langle\langle 2 \rangle^{b'^*|c} \rangle$). Similarly, in the case of 4 subevents, instead of taking twice the product of 2-particle correlators, we have incorporated two different choices ($\langle\langle 2 \rangle^{a'|c^*} \rangle \cdot \langle\langle 2 \rangle^{b|d^*} \rangle$ and $\langle\langle 2 \rangle^{a'|d^*} \rangle \cdot \langle\langle 2 \rangle^{b|c^*} \rangle$) as

$$d_n\{4\}_{4sub} = \langle\langle 4 \rangle^{a'|b|c^*|d^*} \rangle - \langle\langle 2 \rangle^{a'|c^*} \rangle \cdot \langle\langle 2 \rangle^{b|d^*} \rangle - \langle\langle 2 \rangle^{a'|d^*} \rangle \cdot \langle\langle 2 \rangle^{b|c^*} \rangle. \tag{8}$$

The $v_n\{4\}$ value can then be expressed as

$$v_n\{4\} = -d_n\{4\}/(-c_n\{4\})^{3/4}, \tag{9}$$

where $c_n\{4\}$ is the integral cumulant for RFPs.

The systematic uncertainties are evaluated as functions of p_T by using alternative procedures for extracting the cumulants. We take into account the statistical fluctuations in estimating the systematic uncertainties. Systematic uncertainties due to tracking inefficiency and falsely reconstructed track rate are studied by varying the track quality requirements. The selection thresholds on the significances of the transverse and longitudinal track impact parameters divided by their uncertainties are varied from 2 to 5. In addition, the upper limit on the relative p_T uncertainty is varied from 5 to 10% and 15% for pPb and PbPb, respectively. The resulting systematic uncertainty is from 0.03% to 5%, depending on multiplicity, p_T, and collision system. The sensitivity of the results to the primary vertex position along the beam axis (z_{vtx}) is determined by comparing events with different z_{vtx} locations from -15 to $+15$ cm. This systematic uncertainty is estimated to be in range of 0.06%-0.2%, depending on multiplicity, p_T and collision systems. The impact of pileup in pPb collisions is considered by varying the pileup selection of events in the performed analysis by considering the distance among reconstructed vertices and its associated number of tracks. The systematic uncertainty associated with pileup ranges from 0.03% to 0.1%, depending on multiplicity and p_T. Systematic effects from event selections in PbPb are explored by comparing results obtained with and without the requirement of the coincidence of HF calorimeter tower signals above the threshold. This results in a systematic uncertainty of 0.07% for one p_T bin ($8.0 < p_T < 10.0$ GeV), only. Systematic uncertainties originating from different sources are added in quadrature to obtain the total systematic uncertainty shown as boxes in the figures. The systematic uncertainties are common to all methods discussed in this paper. Indeed, the subevent method is just an extension of the standard cumulant calculation and all experimental effects should be the same. So considering lower statistics for subevent cumulants, systematic uncertainty for subevent results have been assumed to be the same as for standard (without subevent) results.

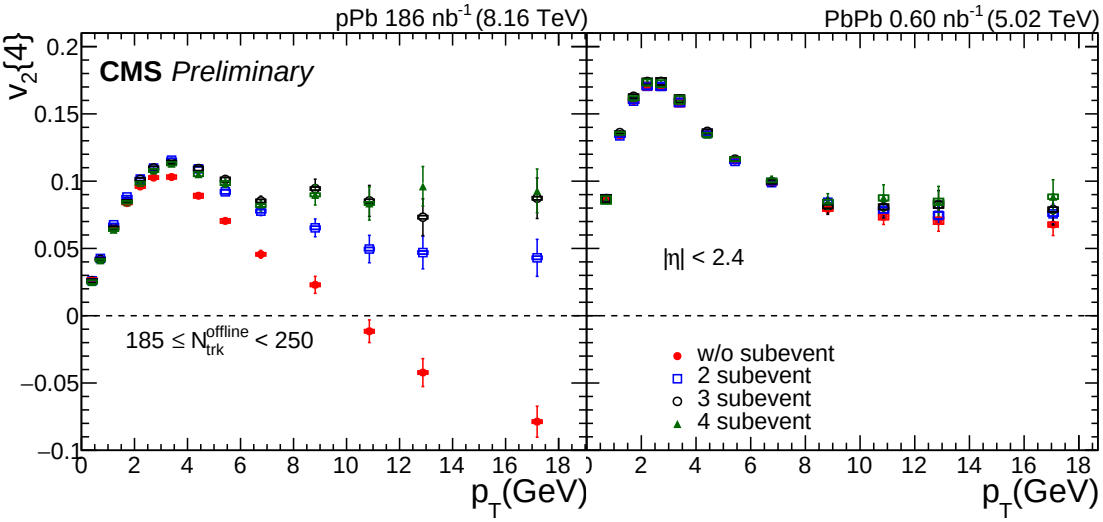

Figure 2: $v_2\{4\}$ vs p_T in $185 \le N_{trk}^{offline} < 250$ for pPb (Left) and PbPb (Right). Statistical uncertainty is represented by solid lines and systematic uncertainty by boxes.

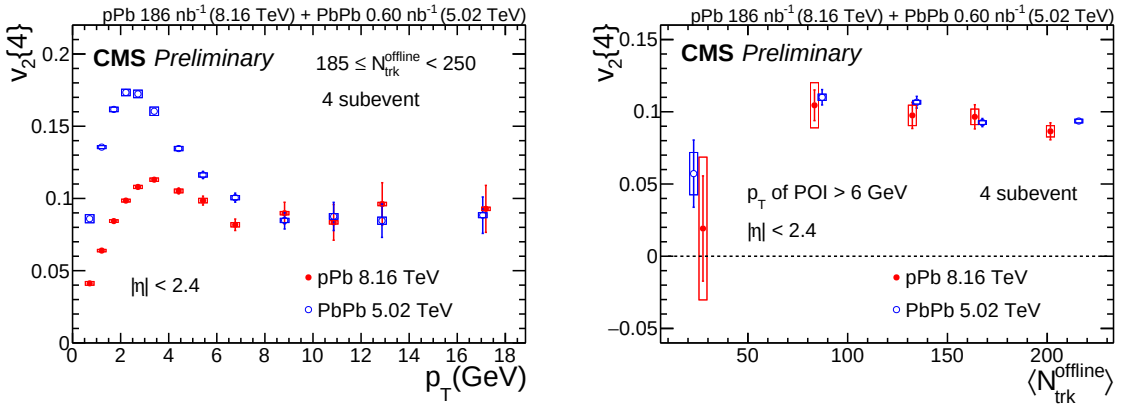

Figure 3: Left: Comparison of $v_2\{4\}$ with 4 subevent vs p_T in $185 \leq \mathrm{N}_{\mathrm{trk}}^{\mathrm{offline}} < 250$ between pPb and PbPb. Right: Comparison of $v_2\{4\}$ with 4 subevent vs $\langle \mathrm{N}_{\mathrm{trk}}^{\mathrm{offline}} \rangle$ for p_{T} of POI > 6 GeV between pPb and PbPb. Statistical uncertainty is represented by solid lines and systematic uncertainty by boxes.

The $v_2\{4\}$ results for the different subevent scenarios are shown for the $185 \leq \mathrm{N}_{\mathrm{trk}}^{\mathrm{offline}} < 250$ range as a function of p_T in Fig. 2. The left panel shows the results for pPb collisions and the right panel for PbPb collisions. The standard $v_2\{4\}$ result (without subevents) goes negative after $p_{\mathrm{T}} \sim 10$ GeV for pPb collisions, which is not the case for the PbPb results. This could be a consequence of selecting rare high multiplicity events in the pPb events with an increased nonflow contribution from jets as compared to PbPb events. Using the subevent method, this negative trend is heavily suppressed and we get positive values of $v_2\{4\}$ (negative value of $d_2\{4\}$) up to $p_{\mathrm{T}} \sim 17$ GeV, the upper limit of the current investigation. The 3 and 4 subevent results are in agreement, suggesting complete removal of non-flow correlations. Also, 3 and 4 subevent $v_2\{4\}$ values are almost constant above $p_{\mathrm{T}} \sim 6$ GeV in both collision systems. The left plot in Fig. 3 compares the 4-subevent, $v_2\{4\}$ values as a function of p_T for pPb and PbPb collisions. We observe similar magnitude of $v_2\{4\}$ in both the collision systems at high p_{T}. In the right plot of Fig. 3, we show the 4-subevent, $v_2\{4\}$ values for POI particles with $p_{\mathrm{T}} > 6\,\mathrm{GeV}$ as a function $\langle \mathrm{N}_{\mathrm{trk}}^{\mathrm{offline}} \rangle$ for pPb and PbPb collisions. The magnitude and $\langle \mathrm{N}_{\mathrm{trk}}^{\mathrm{offline}} \rangle$ dependence of the $v_2\{4\}$ values for the two systems are very similar. Figure 4 of Appendix A shows the $v_2\{4\}$ results in terms of efficiency corrected mean multiplicity ($\langle \mathrm{N}_{\mathrm{trk}}^{\mathrm{corrected}} \rangle$). For the $0 < \mathrm{N}_{\mathrm{trk}}^{\mathrm{offline}} < 60$ range, the $v_2\{4\}$ value is consistent with zero for pPb collisions, within the statistical and systematic uncertainties.

In summary, the $v_2\{4\}$ values calculated using subevents are presented for pPb and PbPb collisions at $\sqrt{s_{\mathrm{NN}}} = 8.16\,\mathrm{TeV}$ and $\sqrt{s_{\mathrm{NN}}} = 5.02\,\mathrm{TeV}$, respectively. This analysis investigates an extended phase space region that has not been previously studied in small systems. After using a subevent method to remove nonflow correlations due to jet fragmentation, a significant and positive value for $v_n\{4\}$ is determined for higher multiplicity pPb events extending to high particle p_{T}. A striking similarity is observed in the magnitudes of high p_{T} $v_2\{4\}$ values in high multiplicity pPb and peripheral PbPb collisions, suggesting a similar mechanism for the observed anisotropy at high p_{T} in the two systems. These results provide new information on the interaction of high-p_{T} partons with the surrounding medium in heavy ion collisions.

References

[1] STAR Collaboration, "Distributions of charged hadrons associated with high transverse momentum particles in pp and AuAu collisions at $\sqrt{s_{\rm NN}} = 200\,\text{GeV}$", *Phys. Rev. Lett.* **95** (2005) 152301, doi:10.1103/PhysRevLett.95.152301, arXiv:nucl-ex/0501016.

[2] STAR Collaboration, "Long-range rapidity correlations and jet production in high energy nuclear collisions", *Phys. Rev. C* **80** (2009) 064912, doi:10.1103/PhysRevC.80.064912, arXiv:0909.0191.

[3] PHOBOS Collaboration, "High transverse momentum triggered correlations over a large pseudorapidity acceptance in AuAu collisions at $\sqrt{s_{\rm NN}} = 200\,\text{GeV}$", *Phys. Rev. Lett.* **104** (2010) 062301, doi:10.1103/PhysRevLett.104.062301, arXiv:0903.2811.

[4] CMS Collaboration, "Long-range and short-range dihadron angular correlations in central PbPb collisions at a nucleon-nucleon center of mass energy of 2.76 TeV", *JHEP* **07** (2011) 076, doi:10.1007/JHEP07(2011)076, arXiv:1105.2438.

[5] CMS Collaboration, "Centrality dependence of dihadron correlations and azimuthal anisotropy harmonics in PbPb collisions at $\sqrt{s_{\rm NN}} = 2.76$ TeV", *Eur. Phys. J. C* **72** (2012) 2012, doi:10.1140/epjc/s10052-012-2012-3, arXiv:1201.3158.

[6] ALICE Collaboration, "Elliptic flow of charged particles in PbPb collisions at 2.76 TeV", *Phys. Rev. Lett.* **105** (2010) 252302, doi:10.1103/PhysRevLett.105.252302, arXiv:1011.3914.

[7] ATLAS Collaboration, "Measurement of the azimuthal anisotropy for charged particle production in $\sqrt{s_{\rm NN}} = 2.76$ TeV lead-lead collisions with the ATLAS detector", *Phys. Rev. C* **86** (2012) 014907, doi:10.1103/PhysRevC.86.014907, arXiv:1203.3087.

[8] CMS Collaboration, "Measurement of the elliptic anisotropy of charged particles produced in PbPb collisions at $\sqrt{s_{\rm NN}} = 2.76$ TeV", *Phys. Rev. C* **87** (2013) 014902, doi:10.1103/PhysRevC.87.014902, arXiv:1204.1409.

[9] CMS Collaboration, "Studies of azimuthal dihadron correlations in ultra-central PbPb collisions at $\sqrt{s_{\rm NN}} = 2.76$ TeV", *JHEP* **02** (2014) 088, doi:10.1007/JHEP02(2014)088, arXiv:1312.1845.

[10] J.-Y. Ollitrault, "Anisotropy as a signature of transverse collective flow", *Phys. Rev. D* **46** (1992) 229, doi:10.1103/PhysRevD.46.229.

[11] U. Heinz and R. Snellings, "Collective flow and viscosity in relativistic heavy-ion collisions", *Ann. Rev. Nucl. Part. Sci.* **63** (2013) 123, doi:10.1146/annurev-nucl-102212-170540, arXiv:1301.2826.

[12] C. Gale, S. Jeon, and B. Schenke, "Hydrodynamic modeling of heavy-ion collisions", *Int. J. Mod. Phys. A* **28** (2013) 1340011, doi:10.1142/S0217751X13400113, arXiv:1301.5893.

[13] B. Schenke, S. Jeon, and C. Gale, "Elliptic and triangular flow in event-by-event (3+1)D viscous hydrodynamics", *Phys. Rev. Lett.* **106** (2011) 042301, doi:10.1103/PhysRevLett.106.042301, arXiv:1009.3244.

[14] Z. Qiu, C. Shen, and U. Heinz, "Hydrodynamic elliptic and triangular flow in PbPb collisions at $\sqrt{s_{\rm NN}} = 2.76$ TeV", *Phys. Lett. B* **707** (2012) 151, doi:10.1016/j.physletb.2011.12.041, arXiv:1110.3033.

[15] CMS Collaboration, "Observation of long-range near-side angular correlations in proton-lead collisions at the LHC", *Phys. Lett. B* **718** (2013) 795, doi:10.1016/j.physletb.2012.11.025, arXiv:1210.5482.

[16] ALICE Collaboration, "Long-range angular correlations on the near and away side in pPb collisions at $\sqrt{s_{\rm NN}} = 5.02$ TeV", *Phys. Lett. B* **719** (2013) 29, doi:10.1016/j.physletb.2013.01.012, arXiv:1212.2001.

[17] ATLAS Collaboration, "Observation of associated near-side and away-side long-range correlations in $\sqrt{s_{\rm NN}} = 5.02$ TeV proton-lead collisions with the ATLAS detector", *Phys. Rev. Lett.* **110** (2013) 182302, doi:10.1103/PhysRevLett.110.182302, arXiv:1212.5198.

[18] LHCb Collaboration, "Measurements of long-range near-side angular correlations in $\sqrt{s_{\rm NN}} = 5$ TeV proton-lead collisions in the forward region", *Phys. Lett. B* **762** (2016) 473, doi:10.1016/j.physletb.2016.09.064, arXiv:1512.00439.

[19] PHENIX Collaboration, "Measurement of long-range angular correlation and quadrupole anisotropy of pions and (anti)protons in central d+Au collisions at $\sqrt{s_{\rm NN}} = 200$ GeV", *Phys. Rev. Lett.* **114** (2015) 192301, doi:10.1103/PhysRevLett.114.192301, arXiv:1404.7461.

[20] STAR Collaboration, "Long-range pseudorapidity dihadron correlations in d+Au collisions at $\sqrt{s_{\rm NN}} = 200$ GeV", *Phys. Lett. B* **747** (2015) 265, doi:10.1016/j.physletb.2015.05.075, arXiv:1502.07652.

[21] PHENIX Collaboration, "Measurements of elliptic and triangular flow in high-multiplicity ^{3}He+Au collisions at $\sqrt{s_{\rm NN}} = 200$ GeV", *Phys. Rev. Lett.* **115** (2015) 142301, doi:10.1103/PhysRevLett.115.142301, arXiv:1507.06273.

[22] J. L. Nagle and W. A. Zajc, "Small system collectivity in relativistic hadronic and nuclear collisions", *Ann. Rev. Nucl. Part. Sci.* **68** (2018) 211, doi:10.1146/annurev-nucl-101916-123209, arXiv:1801.03477.

[23] R. C. Hwa and C. B. Yang, "Recombination of shower partons at high p_T in heavy-ion collisions", *Phys. Rev. C* **70** (Aug, 2004) 024905, doi:10.1103/PhysRevC.70.024905.

[24] C. Marquet, "Large parton densities and high-p(T) physics in heavy-ion collisions", *PoS* **High-pT physics09** (2009) 039, doi:10.22323/1.080.0039, arXiv:0906.3184.

[25] CMS Collaboration, "Azimuthal anisotropy of charged particles at high transverse momenta in pb-pb collisions at $\sqrt{s_{NN}}$=2.76 TeV", *Phys. Rev. Lett.* **109** (Jul, 2012) 022301, doi:10.1103/PhysRevLett.109.022301.

[26] CMS Collaboration, "Azimuthal anisotropy of charged particles with transverse momentum up to 100 GeV/c in PbPb collisions at $\sqrt{s_{\rm NN}} = 5.02$ TeV", *Phys. Lett. B* **776** (2018) 195, doi:10.1016/j.physletb.2017.11.041, arXiv:1702.00630.

[27] R. Nishitani, "Study of azimuthal anisotropy of high-pt charged particles in au au collisions at $\sqrt{s_{\rm NN}}$ = 200 GeV with rhic-phenix", *Proceedings* **10** (2019) doi:10.3390/proceedings2019010042.

[28] STAR, STAR RICH Collaboration, "Azimuthal anisotropy of charged and identified high p(T) hadrons in Au+Au collisions at RHIC", *Nucl. Phys. A* **715** (2003) 737–740, doi:10.1016/S0375-9474(02)01477-X, arXiv:nucl-ex/0210027.

[29] CMS Collaboration, "Evidence for collective multiparticle correlations in pPb collisions", *Phys. Rev. Lett.* **115** (2015) 012301, doi:10.1103/PhysRevLett.115.012301, arXiv:1502.05382.

[30] CMS Collaboration, "Evidence for transverse momentum and pseudorapidity dependent event plane fluctuations in PbPb and pPb collisions", *Phys. Rev. C* **92** (2015), no. 3, 034911, doi:10.1103/PhysRevC.92.034911, arXiv:1503.01692.

[31] ATLAS Collaboration, "Transverse momentum and process dependent azimuthal anisotropies in $\sqrt{s_{\mathrm{NN}}} = 8.16$ TeV p+Pb collisions with the ATLAS detector", *Eur. Phys. J. C* **80** (2020), no. 1, 73, doi:10.1140/epjc/s10052-020-7624-4, arXiv:1910.13978.

[32] ALICE Collaboration, "Azimuthal anisotropy of jet particles in p-Pb and Pb-Pb collisions at $\sqrt{s_{\mathrm{NN}}} = 5.02$ TeV", arXiv:2212.12609.

[33] ATLAS Collaboration, "Measurements of long-range azimuthal anisotropies and associated Fourier coefficients for pp collisions at $\sqrt{s} = 5.02$ and 13 TeV and p+Pb collisions at $\sqrt{s_{\mathrm{NN}}} = 5.02$ TeV with the ATLAS detector", *Phys. Rev. C* **96** (2017), no. 2, 024908, doi:10.1103/PhysRevC.96.024908, arXiv:1609.06213.

[34] A. Bilandzic, R. Snellings, and S. Voloshin, "Flow analysis with cumulants: Direct calculations", *Phys. Rev. C* **83** (2011) 044913, doi:10.1103/PhysRevC.83.044913, arXiv:1010.0233.

[35] P. Di Francesco, M. Guilbaud, M. Luzum, and J.-Y. Ollitrault, "Systematic procedure for analyzing cumulants at any order", *Phys. Rev. C* **95** (2017) 044911, doi:10.1103/PhysRevC.95.044911, arXiv:1612.05634.

[36] J. Jia, M. Zhou, and A. Trzupek, "Revealing long-range multiparticle collectivity in small collision systems via subevent cumulants", *Phys. Rev. C* **96** (2017) 034906, doi:10.1103/PhysRevC.96.034906, arXiv:1701.03830.

[37] CMS Collaboration, "Track impact parameter resolution for the full pseudorapidity coverage in the 2017 dataset with the CMS Phase-1 pixel detector", CMS Physics Analysis Summary CMS-DP-2020-049, 2020.

[38] CMS Collaboration, "Description and performance of track and primary-vertex reconstruction with the CMS tracker", *JINST* **9** (2014) P10009, doi:10.1088/1748-0221/9/10/P10009, arXiv:1405.6569.

[39] CMS Collaboration, "The CMS experiment at the CERN LHC", *JINST* **3** (2008) S08004, doi:10.1088/1748-0221/3/08/S08004.

[40] CMS Collaboration, "CMS luminosity measurement using 2016 proton-nucleus collisions at nucleon-nucleon center-of-mass energy of 8.16 TeV", CMS Physics Analysis Summary CMS-PAS-LUM-17-002, 2018.

[41] CMS Collaboration, "CMS luminosity measurement using nucleus-nucleus collisions at $\sqrt{s_{_{\mathrm{NN}}}} = 5.02$ TeV in 2018", CMS Physics Analysis Summary CMS-PAS-LUM-18-001, 2022.

[42] CMS Collaboration, "Performance of the CMS Level-1 trigger in proton-proton collisions at $\sqrt{s} = 13$ TeV", *JINST* **15** (2020) P10017, doi:10.1088/1748-0221/15/10/P10017, arXiv:2006.10165.

[43] CMS Collaboration, "The CMS trigger system", *JINST* **12** (2017) 01020, doi:10.1088/1748-0221/12/01/P01020, arXiv:1609.02366.

[44] CMS Collaboration, "Multiplicity and transverse momentum dependence of two- and four-particle correlations in pPb and PbPb collisions", *Phys. Lett. B* **724** (2013) 213, doi:10.1016/j.physletb.2013.06.028, arXiv:1305.0609.

[45] CMS Collaboration, "Evidence for collectivity in pp collisions at the LHC", *Phys. Lett. B* **765** (2017) 193, doi:10.1016/j.physletb.2016.12.009, arXiv:1606.06198.

[46] CMS Collaboration, "Multiparticle correlation studies in pPb collisions at $\sqrt{s_{\mathrm{NN}}} = 8.16$ TeV", *Phys. Rev. C* **101** (2020) 014912, doi:10.1103/PhysRevC.101.014912, arXiv:1904.11519.

[47] M. Gyulassy and X.-N. Wang, "HIJING 1.0: A Monte Carlo program for parton and particle production in high-energy hadronic and nuclear collisions", *Comput. Phys. Commun.* **83** (1994) 307, doi:10.1016/0010-4655(94)90057-4, arXiv:nucl-th/9502021.

[48] I. P. Lokhtin and A. M. Snigirev, "A model of jet quenching in ultrarelativistic heavy ion collisions and high-p_{T} hadron spectra at RHIC", *Eur. Phys. J. C* **45** (2006) 211, doi:10.1140/epjc/s2005-02426-3, arXiv:hep-ph/0506189.

[49] GEANT4 Collaboration, "GEANT4–a simulation toolkit", *Nucl. Instrum. Meth. A* **506** (2003) 250, doi:10.1016/S0168-9002(03)01368-8.

[50] A. Bilandzic et al., "Generic framework for anisotropic flow analyses with multiparticle azimuthal correlations", *Phys. Rev. C* **89** (2014) 064904, doi:10.1103/PhysRevC.89.064904, arXiv:1312.3572.

[51] CMS Collaboration, "Multiparticle correlation studies in pPb collisions at $\sqrt{s_{\mathrm{NN}}} = 8.16$ TeV", *Phys. Rev. C* **101** (2020) 014912, doi:10.1103/PhysRevC.101.014912, arXiv:1904.11519.

[52] CMS Collaboration, "Pseudorapidity and transverse momentum dependence of flow harmonics in pPb and PbPb collisions", *Phys. Rev. C* **98** (2018) 044902, doi:10.1103/PhysRevC.98.044902, arXiv:1710.07864.

A Supplemental material

A.1 Mapping between $N_{trk}^{offline}$ and $N_{trk}^{corrected}$ in pPb and PbPb collisions

Table A.1: Average multiplicity $\langle N_{trk}^{offline} \rangle$ and tracking efficiency corrected multiplicity $\langle N_{trk}^{corrected} \rangle$ in various $N_{trk}^{offline}$ bin is given below.

	pPb		PbPb	
$N_{trk}^{offline}$ range	$\langle N_{trk}^{offline} \rangle$	$\langle N_{trk}^{corrected} \rangle$	$\langle N_{trk}^{offline} \rangle$	$\langle N_{trk}^{corrected} \rangle$
$(0, 60)$	27	33±1	23	39±2
$[60, 120)$	83	101±4	87	152±6
$[120, 150)$	132	160±6	135	233±10
$[150, 185)$	164	198±7	168	287±12
$[185, 250)$	202	245±10	216	368±16

A.2 Right plot of Figure 3 with $\langle N_{trk}^{corrected} \rangle$ on x-axis

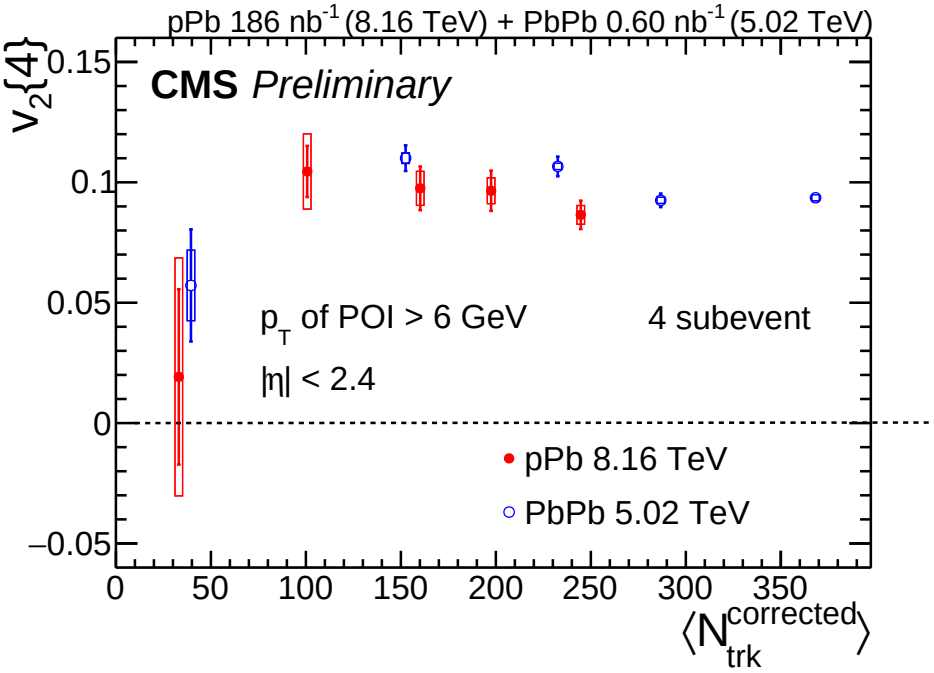

Figure 4: Comparison of $v_2\{4\}$ values with $p_T^{POI} > 6\,GeV$ based on the 4-subevent method as a function of $\langle N_{trk}^{corrected} \rangle$ between pPb and PbPb. The solid lines and boxes indicate the statistical and systematic uncertainties, respectively.